Bilayer Graphene Growth by Low Pressure Chemical Vapor Deposition on Copper Foil

by

Wenjing Fang

B.Eng., Nanyang Technological University (2010)

Submitted to the Department of Electrical Engineering and Computer Science

in Partial Fulfillment of the Requirements for the Degree of

Master of Science

at the

Massachusetts Institute of Technology

June 2012

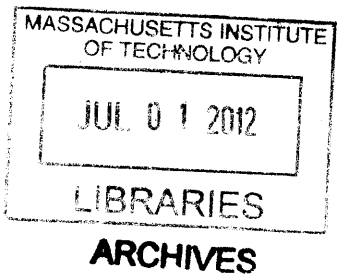

Author_____

Department of Electrical Engineering and Computer Science

May 23, 2012

Certified by_____

Jing Kong

ITT Career Development Associate Professor of Engineering and Computer Science

Thesis Supervisor

Accepted by_____

Leslie A. Kolodziejski

Chair, Department Committee on Graduate Students

(This page is left intentionally blank)

Bilayer Graphene Growth by Low Pressure Chemical Vapor Deposition on Copper Foil

by

Wenjing Fang

Submitted to the
Department of Electrical Engineering and Computer Science

May 23, 2012

In Partial Fulfillment of the Requirements for the Degree of
Master of Science in Electrical Engineering and Computer Science

ABSTRACT

Successfully integrating graphene in standard processes for applications in electronics relies on the synthesis of high-quality films. In this work we study Low Pressure Chemical Vapor Deposition (LPCVD) growth of bilayer graphene on the outside surface of copper enclosures. The effect of several parameters on bilayer growth rate and domain size was investigated and high-coverage bilayers films were successfully grown. Furthermore, the quality of the bilayer was confirmed using Raman spectroscopy. Finally, we consider future studies that may reveal the underlying mechanisms behind bilayer growth.

Thesis Supervisor: Jing Kong
Title: Associate Professor, MIT Electrical Engineering and Computer Science

Acknowledgements

I would like to thank Professor Mildred Dresselhaus and Professor Jing Kong for offering me the opportunities to do research in their groups, especially for Professor Jing Kong's supervision and guidance throughout the process of completing this thesis, without which this would not have been possible. I would like to thank all the lab mates for their help, support and friendship during my time in the NME (Nano-Materials and Electronics) group at MIT. Lastly, I would like to thank my parents for their unconditional love.

Contents

List of Figures

1. Introduction to Graphene

Graphene, a single layer of sp^2-bonded hexagonal carbon structure, has attracted a great deal of attention since its discovery. [1] Graphene possesses exceptional electronic, thermal and mechanical properties.[2-4] The unique electronic properties of graphene have sparked tremendous interest in its potential for future electronic applications such as high-speed radio frequency devices, nanoelectronics, and bioelectronics. [5-8] Also, graphene films can serve as transparent electrode materials in solar cells, liquid crystal devices and ultra-capacitors. [9, 10]

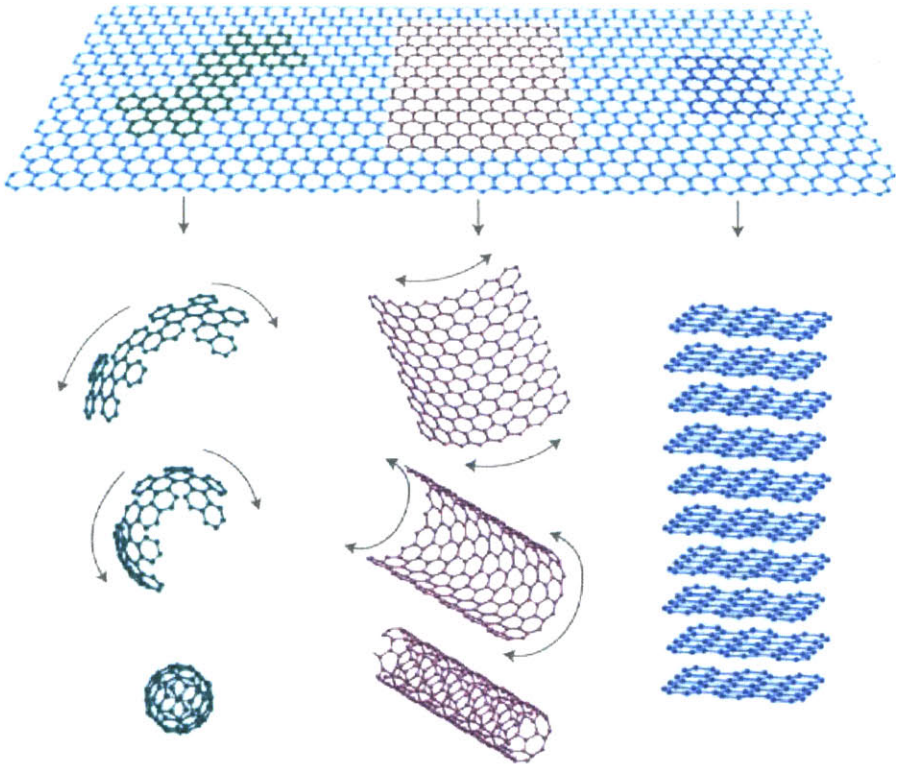

Figure 1. Graphene is the building block for carbon materials of all other dimensionalities: 0D buckyballs, 1D nanotubes and 3D graphite. [11]

To realize these applications, reproducibly fabricating high-quality graphene in large quantities is of paramount importance. Various approaches have been developed to produce single or few-layer graphene, such as epitaxial growth[12, 13], chemical reduction of graphene oxides[14], and chemical vapor deposition (CVD). [15-17] Among them, CVD growth is most suitable for preparing large area and high quality graphene films. Reina et al. have demonstrated that single and few-layered graphene films can be synthesized on the surface of polycrystalline Ni by CVD. [15, 16] More recent reports have shown that single layer graphene films can grow on Cu. [17] Additionally, graphene or graphite film growth on non-noble metals such as Fe and Co has been reported. [18]

The CVD process for graphene growth with dissolution-precipitation mechanism can be described as follows: the reactive carbon species are generated at the metal surface by decomposing hydrocarbon gas, a concentration gradient results causing carbon atoms to diffuse into the metal. It is known that the solubility of carbon in a metal increases with temperature. For instance, pure Ni dissolves ~1.3 atom % of carbon at 1000°C. Some of the carbon atoms dissolved in a metal at high temperature can precipitate as a graphite film upon cooling. Reina et al. has demonstrated that thin Ni films and fast-cooling processes have been used to suppress the amount of precipitated carbon.[19] However, these methods yield non-uniform graphene because multi-layer graphene films preferentially precipitate at the metal grain boundaries. In contrast, due to low carbon solubility in Cu, large-area monolayer graphene can be synthesized on Cu by self-limiting surface deposition[17].

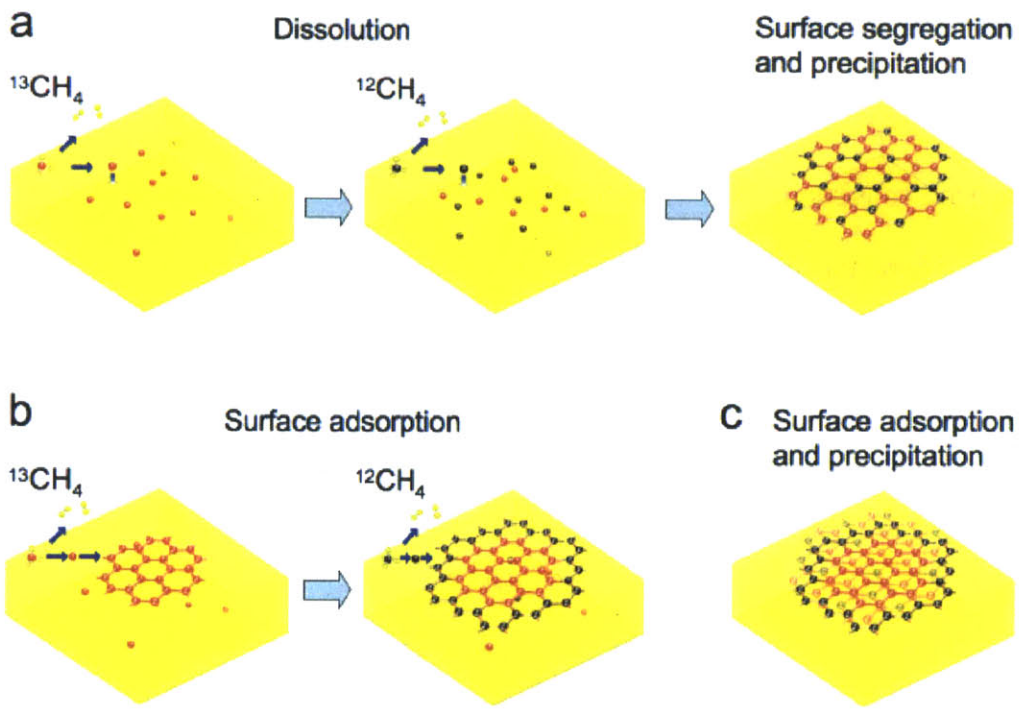

Figure 2. Different growth mechanisms for graphee films grown on Ni and Cu substrate. [20]

Li et al. also showed the differences between the graphene growth mechanisms on Ni and Cu at the same temperature.[20] It was demonstrated that at elevated temperatures (~1000°C), graphene on Ni was grown by carbon segregation from the bulk whereas those grown on Cu grew from carbon atoms adsorbed on the Cu surface. By switching the hydrocarbon source between C^{12} and C^{13} isotope labeled CH_4 during the growth stage, spatial distributions of the carbon isotopes forming the graphene could be identified by mapping the Raman G band frequency from of the graphene surface. If the growth of graphene occurred due to the dissolution-precipitation mechanism, it was expected that mixing of the carbon isotopes occurred in the bulk and the resulting graphene would be formed of randomly distributed carbon isotopes. While the on the graphene film grown on Cu, spatial distribution of the carbon isotopes were observed, indicating the surface adsorption mechanism.

1.1 Properties and Fabrication of Bilayer Graphene

1.1.1 Structure of Bilayer Graphene

Bilayer graphene consists of two layers of monolayer graphene. It is found in either a twisted configuration, where the two layers are relatively rotated (Figure 3c) or a graphitic Bernal stacked configuration where half the atoms in one layer lie atop half the atoms in the other (Figure 3b). Stacking order and orientation greatly influence the optical and electronic properties.

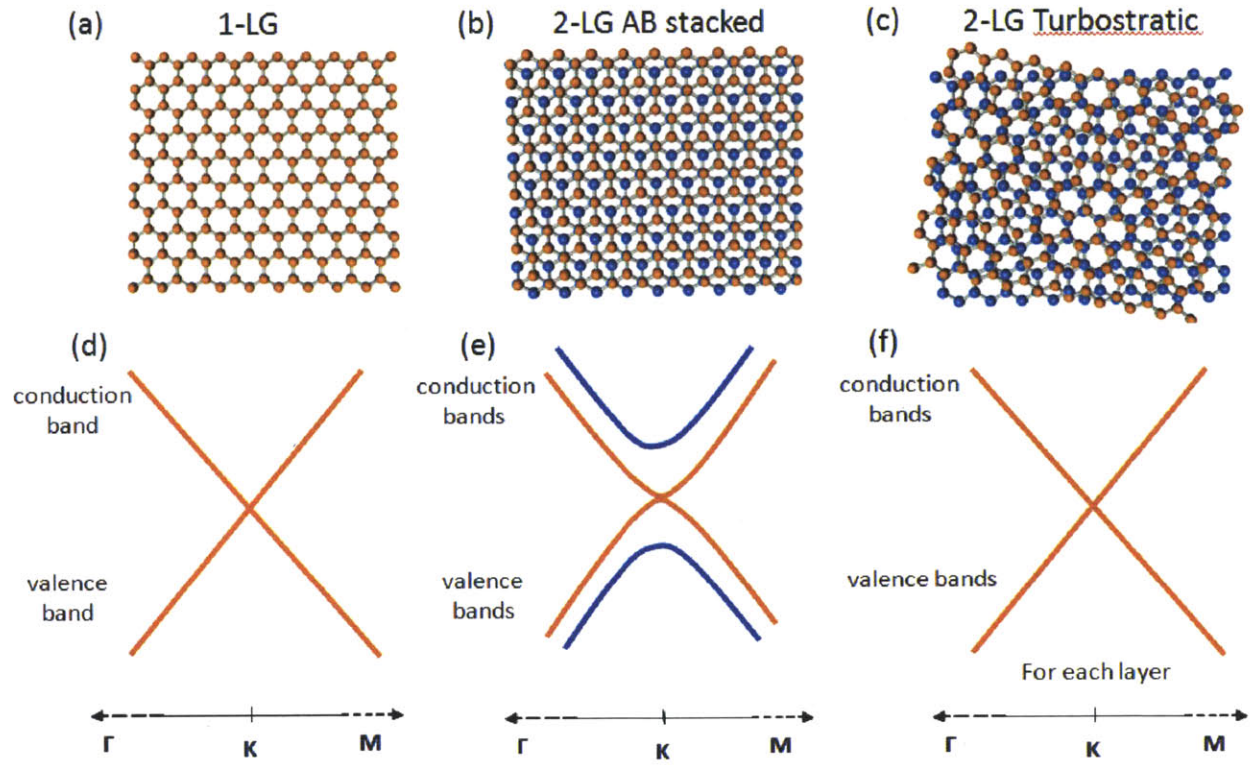

Figure 3. Stacking order of bilayer graphene and its band structure.

Bilayer graphene has been widely studied recently and has been suggested for applications in electronic devices. For instance, Bernal-stacked bilayers can exhibit a tunable bandgap of up to 250 mV by an external electric field, [23] — making it a promising candidate for transistors or nano-electronic applications.[21, 22] Attention has also been given to the misoriented bilayer; the orientation of the layers give rise to different inter-layer interactions, which may have

applications in BISFETs. [24] This new transistor architecture takes special advantage of the bilayer's unique properties.

Another promising application of graphene is as a transparent conductive electrode because of its high optical transmittance and electrical conductivity. The sheet resistance of a monolayer graphene is about 900Ω/sq[25], which is considered fairly high for electrodes. Several papers report stacked multilayers by transferring monolayer graphene sequentially.[26] However, this method requires considerable time and effort. In addition, the average transmittance per layer decreases as number of layers increases due to cracks, wrinkles and residues introduced during the transfer process. Direct synthesis of bilayer graphene can help minimize the number of transfers, thus simplify the process. High quality and uniformity is expected of bilayer graphene used as transparent electrode not only for better electrical performance, but also for mechanical robustness.

1.2 Characterization of Bilayer Graphene

1.2.1 Optical microscopy

Optical microscopy is used to examine the surface morphology of graphene films on Si/SiO_2 substrate and determine the uniformity and thickness. By using Si substrates with a 300 nm oxide layer, we can observe the change of color contrast in the optical images, indicating variations in the film thickness, due to light interference on the SiO_2 modulated by the graphene layers.

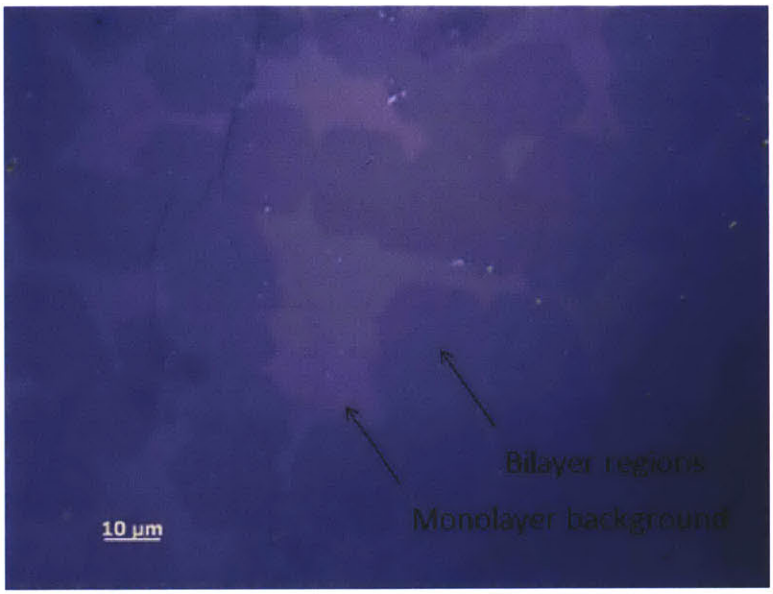

Figure 4. Typical optical images of graphene films on Si wafer with 300 nm thick SiO_2.

Shown in Figure 4, the lightest purple regions in the optical images correspond to monolayer graphene. In contrast, bilayer graphene regions with a hexagonal shape show darker contrast. The white colored text are residues from transfer.

1.2.2 Raman spectroscopy

Raman spectroscopy allows for quick, facile structural and quality characterization. Bernal stacked bilayers show a distinct characteristic: 2D peak splitting. The 2D peak widens with FWHM (full width at half maximum) about 45 to 55 cm^{-1}, which can be fitted into four sub-peaks using Lorentz fitting, with FWHM of about 25 cm^{-1}. The FWHM for CVD graphene is similar compared to the HOPG blayer graphene In Figure 5, which is cited from Yan's paper [27]; we typically observe an asymmetric 2D peak with decreasing 2D/G ratio. While for turbostratic graphene, 2D peak is relatively narrow and the asymmetry of 2D band is absent.

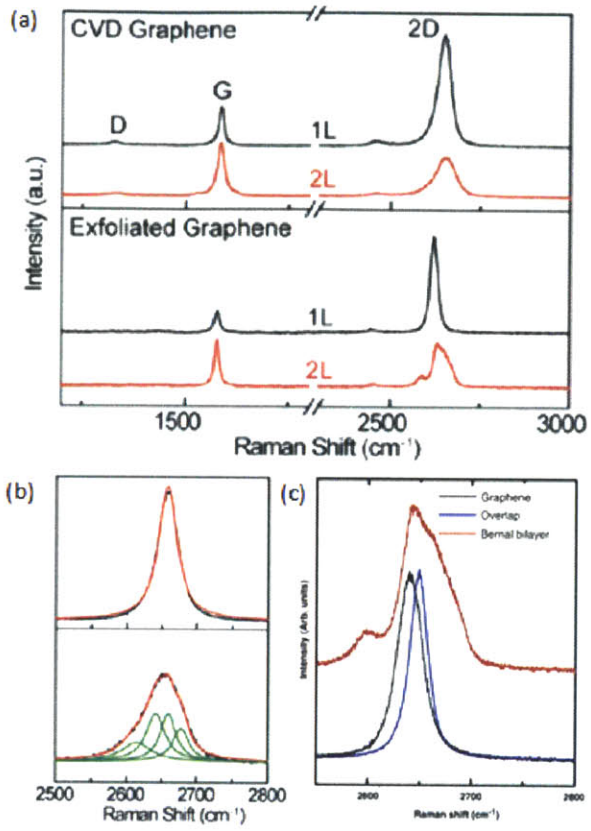

Figure 5. (a).Comparison of Raman spectra of monolayer and bilayer graphene transferred onto SiO_2/Si substrates. (b).Comparison of 2D bands of monolayer and bilayer. (c).Comparison of 2D bands of monolayer graphene, Bernal stacked bilayer and turbostratic bilayer graphene.

1.2.3 Transmission Electron Microscopy

Transmission Electron Microscopy (TEM) provides an accurate way to measure the number of layers and electron diffraction on the graphene film helps reveal the stacking order and domain size. Figure 6 is cited from Yan's paper. [27]

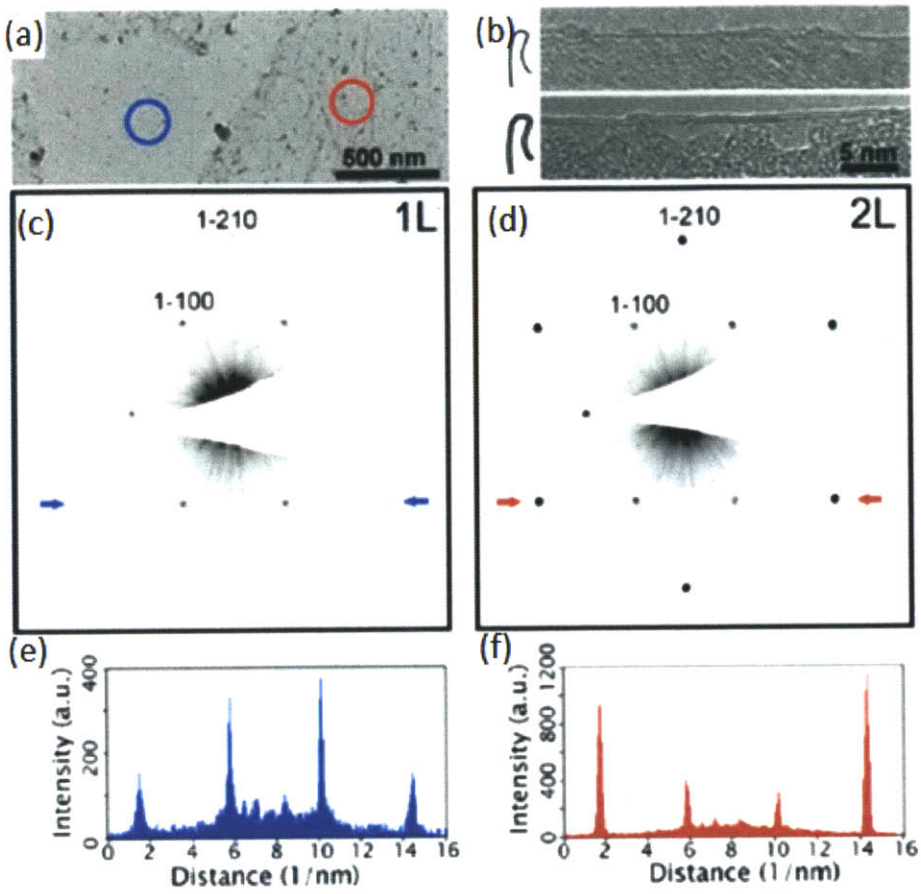

Figure 6: High resolution TEM images and SAED patterns. (a) Bright-field TEM image of as-grown graphene film. The monolayer and bilayer regions are indicated by the blue and red circles, respectively. (b) High-resolution TEM images showing the folded-edges of as-grown graphene films with monolayer and bilayer regions. (c,d) Typical normal incident SAED patterns of monolayer and bilayer regions, respectively. (e,f) Intensity profiles along arrows in (c,d), respectively.

Figure 6 (a) shows that bilayer graphene regions can be distinguished by contrast under high magnification due to the presence of the residues. The edges of the suspended film always fold back, allowing for a cross-sectional view of the film. (Figure 6b) The observation of these edges by TEM provides an accurate way to measure the number of layers at multiple locations on the

film. SAED studies for monolayer and Bernal stacked bilayer generate a single set of hexagon diffraction pattern. To confirm the Bernal stacking, the line profiles of diffraction patterns needs to be analyzed by calculating the intensity ratio of outer peaks from equivalent planes {1-210} over inner peaks from {1-100}. For monolayer graphene, the ratio is below 1. For Bernal stacked bilayers, this ratio is about 2. If there is stacking disorder between the bilayer, we will observe two sets of misaligned electron diffraction spots.

1.2.4 Electrical Measurements

For Bernal stacked bilayer, usually dual-gated graphene field-effect transistors (FETs) are fabricated and electrical measurements are carried out for verification. In 2009, Zhang et al. first demonstrated the realization of a widely tunable electronic band gap in electrically gated bilayer graphene by using a dual-gate bilayer graphene FET and infrared micro-spectroscopy. They reported a gate-controlled, continuously tunable band gap of up to 250 meV. The figure shown below is cited from their paper.[23]

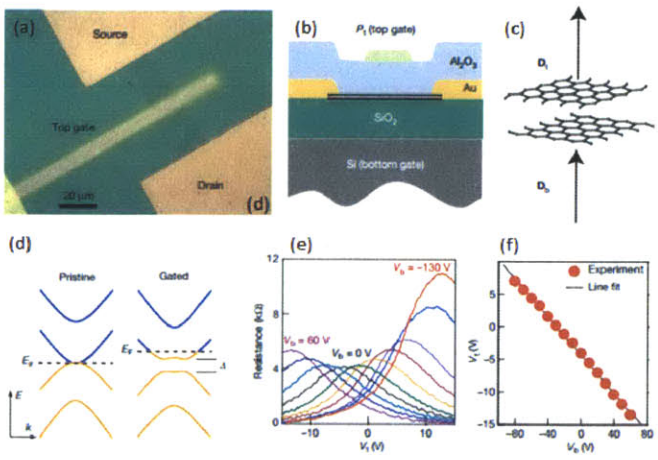

Figure 7. Structure of duel-gated graphene field-effect transistors (FETs) and typical electrical measurement for Bernal stacked bilayer graphene.

In the paper, they demonstrated that by using both top and bottom gates in the graphene FET device, they were able to control independently the two key semiconductor parameters: electronic bandgap and carrier concentration. Figure 7c, explain that gating of the bilayer induces top (D_t and bottom (D_b) electrical displacement fields. Upon electrical gating, the top and bottom electrical displacement fields D_t and D_b produce two effects (Figure. 7d): Tthe difference of the two, $\delta D = D_b - D_t$, leads to a net carrier doping, that is, a shift of the Fermi energy (E_F). The average of the two, $\overline{D} = (D_b + D_t)/2$, breaks the inversion symmetry of the bilayer and generates a non-zero bandgap D. By setting δD to zero and varying $\overline{D}$, the bandgap can be tuned while keeping the bilayer charge neutral. The electronic structure of a pristine bilayer has zero bandgap, while upon gating, the displacement fields induces a non-zero bandgap and a shift of the Fermi energy. The relationship between D and V for the top or bottom layers can be determined through electrical transport measurements and electrical resistance as a function of top gate voltage V_t at different bottom gate voltages V_b. The resistance peak in each curve corresponds to the "charge neutral points" (CNPs) for a given V_b. And there is a linear relation between top and bottom gate voltages that results in bilayer CNPs, as shown in Figure 7f.

1.3 Approaches to Synthesize Bilayer Graphene

Reported prototype Bernal-stacked bilayer graphene transistors were mostly fabricated with mechanical exfoliated graphene films[28], which is difficult to scale and thus not appropriate for mass production. For macroscopic scale studies of bilayer, the "bilayer" is usually made by two consequent transfers of monolayer graphene, which leaves interlayer residues and prevents perfect contact. Therefore, producing large scale graphene with a uniformly controlled number of

layers and stacking order has been extensively studied. One recent advance in growing uniform wafer scale Bernal-stacked bilayer graphene is reported. [30] The author claims homogenous bilayer films with coverage of 99% using LPCVD method by adjusting the cooling rate. However, its mechanism is unclear and the results had not been readily reproduced by other groups. CVD growth on copper substrate results in predominately single layer graphene due to the self-limiting effect.[29] Though multi-layered graphene can be grown on Ni, such films are generally randomly stacked and not uniform in thickness due to the non-equilibrium precipitation of carbon.[14] Since Cu and Ni are well-known binary isomorphous systems, a Cu-Ni alloy would be an ideal system that has moderate solubility that is also controllable by tuning the atomic fraction of Ni in Cu.. Another method with layer control is a segregation approach by combining the different carbon solubilities of Ni and Cu. [31] Recently, Yan et al. has demonstrated a novel vapor-phase epitaxy method by depositing epitaxially another monolayer on an existing monolayer using a two-step growth to achieve Bernal-stacked bilayer graphene.[27] However, this only results in only ~60% bilayer coverage.

1.4 Bilayer Graphene Growth Mechanism

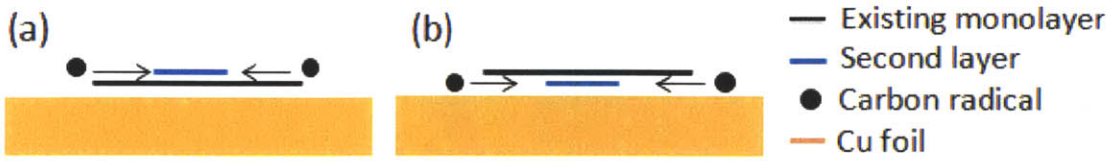

Figure 8. The bilayer graphene growth mechanisms.

A better understanding of how bilayers grow is imperative not only to obtaining homogenous bilayer films but also to eliminating unwanted multilayers in single-layer graphene. It is well known that in crystal growth, new layers nucleate and grow on top of prior layers. While for bilayer growth, it has been shown that the second layer nucleates and grows underneath the first layer on Ir(111), by performing low-energy electron diffraction (LEED) and low-energy electron microscopy (LEEM). [32] They reported that the second graphene growth occurred when carbon was segregating from the Ir substrate or when carbon was deposited on top of the first graphene layer, regardless of whether the substrate is fully covered by graphene films or not. In addition, Nie et al. has demonstrated the under layer growth mechanism for graphene bilayer growth during CVD on Cu foil substrate, though negligible carbon solubility prevents graphene growth by segregation.[33] They observed the new layers nucleate and grow next to the Cu substate, which implies that carbon atoms diffuse along the graphene/Cu interface and incorporate to the existing bilayer underneath. They also proposed that during graphene CVD process, the carbon diffuses to the substrate/film interface, leading to the nucleation and growth of buried layers. This helps explain the "self-limiting" effect that growth from below constrains the ability to make continuous bilayer graphene, that is, underneath grows more slowly than the top one because of its buried edge compared to top layer's exposed edge.

2. Experiment

2.1 Growth of Single Layer Graphene on Copper Foil

Copper foil (purchased from Alfa Aesar) is used as the catalytic substrate to grow monolayer graphene. There are four stages for graphene growth: 1. Ramping up of the temperature, 2. Annealing of the substrate, 3. Graphene growth, 4. Cooling down of the substrate. Copper foil substrate were loaded into the quartz tube and the chamber was purged with H_2 (30%, 10 sccm) for 10 min, followed by ramping the furnace temperature to 1000°C in the same conditions for 20 min. After the temperature reached 1000°C, the H_2 environment was maintained for 30 min to reduce the native copper oxide on the surface of the copper foil. The growth of single layer graphene (SLG) was started by flowing H_2/CH_4 gas mixture. The growth time was about 2 hour. After CVD growth, the furnace was turn off and opened immediately and the copper foil in the quartz tube was cooled down using the same gas composition as growth stage.

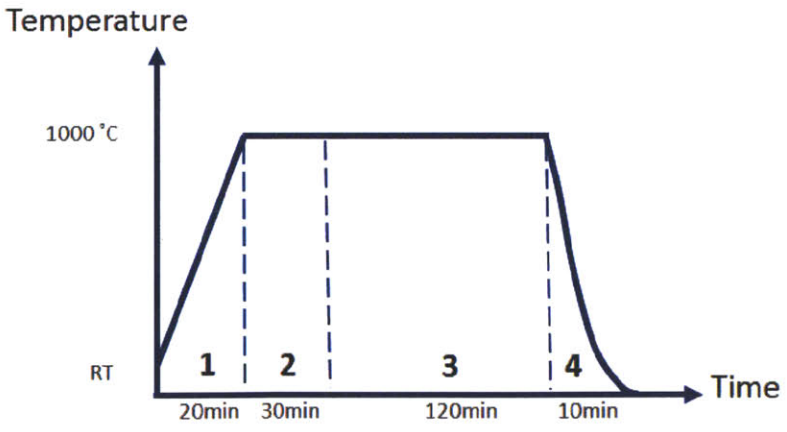

Figure 9. Procedure for graphene growth. There are four stage denoted as the 1.Ramping-up, 2. Annealing, 3. Growth and 4 Cooling down.

2.2 Transfer of graphene films

A thin layer of poly(methyl methacrylate) (PMMA, MicroChem, 950,000 MW, 9.6 wt. % in anisole) was spin-coated on the graphene film and copper substrate at 2500 r.p.m for 1 min. After coating, the sample was annealed at 80°C in ambient for 10 min. The graphene/PMMA stacks were then released by chemically etching the copper using commercial copper etchant. The suspended films were transferred to DI water to remove any residual copper etchant. Subsequently, the graphene/PMMA films were transferred onto desired substrates, such as Si/SiO_2. Finally, the PMMA was dissolved with acetone and the samples were rinsed with deionized water.

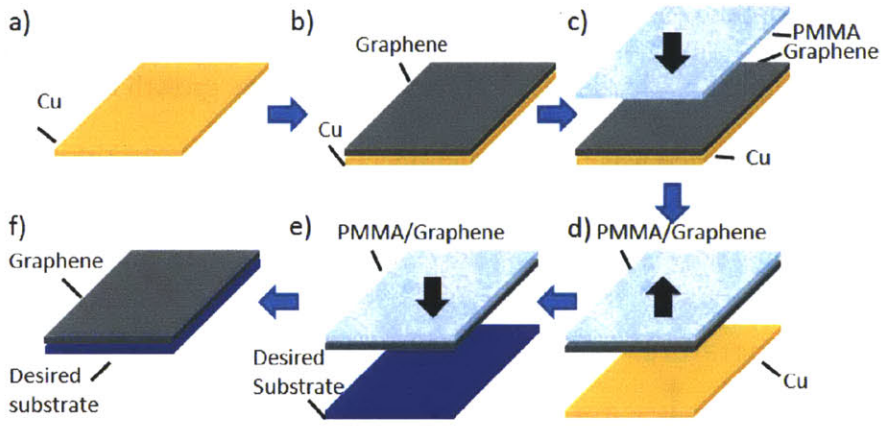

Figure 10. Schematic diagram of graphene transfer process

3. Optimization of Bilayer Growth

Direct synthesis of bilayer graphene can help minimize the number of transfers of monolayer, thus simplify the process for the application of electronic devices or transparent electrodes. High quality and uniformity is expected of bilayer graphene. A uniform and controllable graphene growth is thought to be related to the preparation of the substrate, the distribution and concentration of carbon source, gas composition, growth temperature and total pressure. We will discuss each factor in this section.

3.1. Selection of Substrate

In this experiment, we investigate the growth of bilayer graphene on both flat copper foil and copper foil enclosures. The copper foil enclosure was formed by bending the copper foil and then crimping the three remaining sides. Graphene grows on both the inside and outside of the Cu enclosure. Li et al. showed that graphene with domains of up to 0.5 mm in size was observed on the inside surface. They explained that the low density of nucleation sites is due to the much lower partial pressure of methane and an "improved" environment during growth; that is, the Cu vapor is in a static equilibrium, and there is potentially much lower pressure of unwanted species. At the same time, a higher density of bilayer and/or multi-layer could be observed on the outside of the enclosure at lower methane partial pressures, lower methane flow rates, and longer growth times.

3.1.1 Effect of the Fold

We carried out a time-dependent study by monitoring the growth of graphene on both flat Cu substrates and Cu foil enclosures at 1000°C using 1.5 sccm CH_4 and 35sccm H_2. Both flat and folded substrates were put at the center of the quartz tube for growth at the same time. The flat substrate was put downstream throughout the experiment but the relative positioning of the substrates does not show noticeable difference.

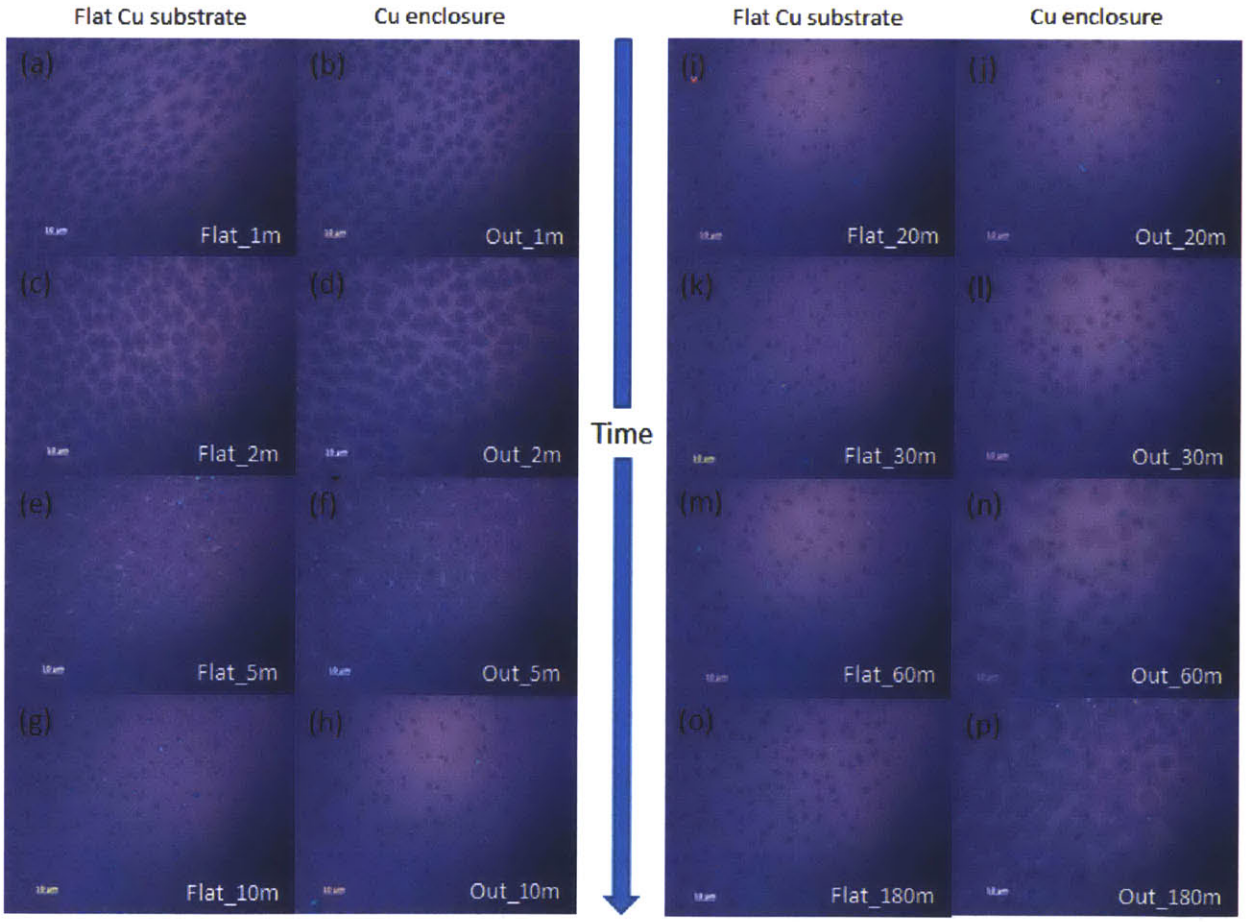

Figure 11. Optical images of graphene films grown on both flat Cu substrates and outside surface of Cu foil enclosures at 1000°C using 1.5sccm CH_4 and 35sccm H_2 as a function of time.

Only the graphene film on the outside surface is compared with that on the flat surface. Since the graphene on the inside surface is in a different environment: the nucleation density is fairly low with much smaller area of bilayer, which will be discussed later. For Figure 11a-f, the monolayer graphene is not complete; while for g-p, there is a monolayer graphene background with darker regions, which indicates the bilayer graphene. As shown in Figure 11a and b, at the early stage of growth (at ~5min), the nucleation density/graphene domain size is similar for both flat Cu substrates and Cu foil enclosures substrates. And we could observe that the monolayer and bilayer graphene nucleate at the same time. It should be noted that once monolayer coverage is complete (~ 10min), the bilayer graphene on outside surface of Cu enclosure continues to grow while on the flat copper, we witness a "self-limited" effect, which is consistent with previous report. Bilayer graphene grows as time increases, but the growth rate on flat substrate is extremely slow compared to that on the enclosure, for which bilayer graphene reached 85% coverage after a 3 hour growth at 1000^{o}C.

The enclosure shape is critical for the growth of bilayer on the outside surface. Other shapes such as a copper foil rolled into a cylinder (Figure 12b) or a copper foil fold without crimping at the edges (c) were used but large bilayer graphene domains could not be observed on either the inside or the outside surface.

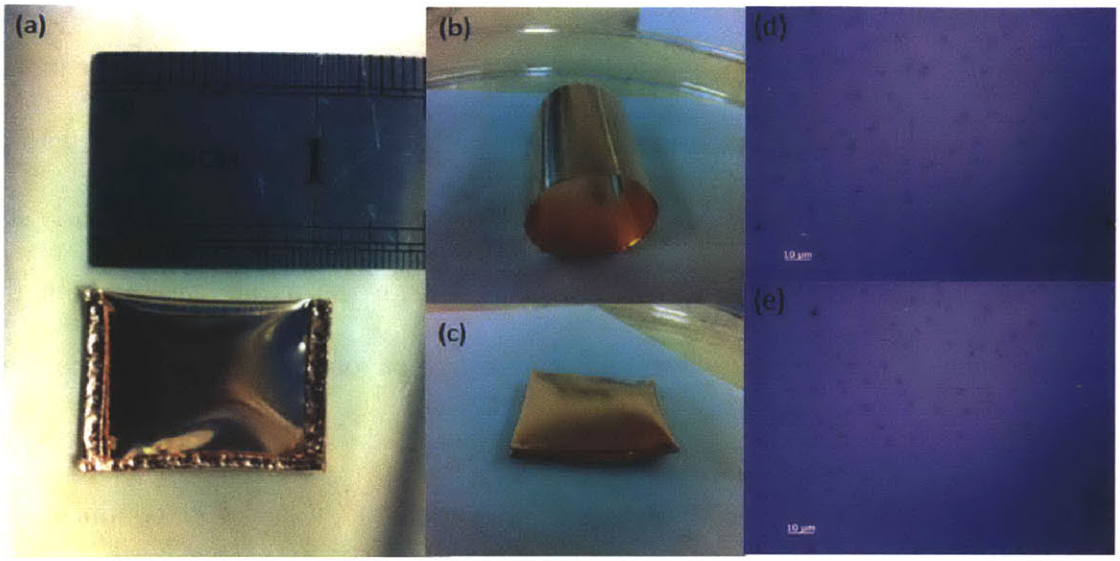

Figure 12. Pictures of different shapes of Cu foils. Cu foil enclosure (a), a copper foil rolled into a cylinder (b) and a copper foil enclosure without crimping at the edges (c). (d) and (e) corresponds to the graphene grown at 1000^0C using 1.5sccm CH_4 and 35sccm H_2.

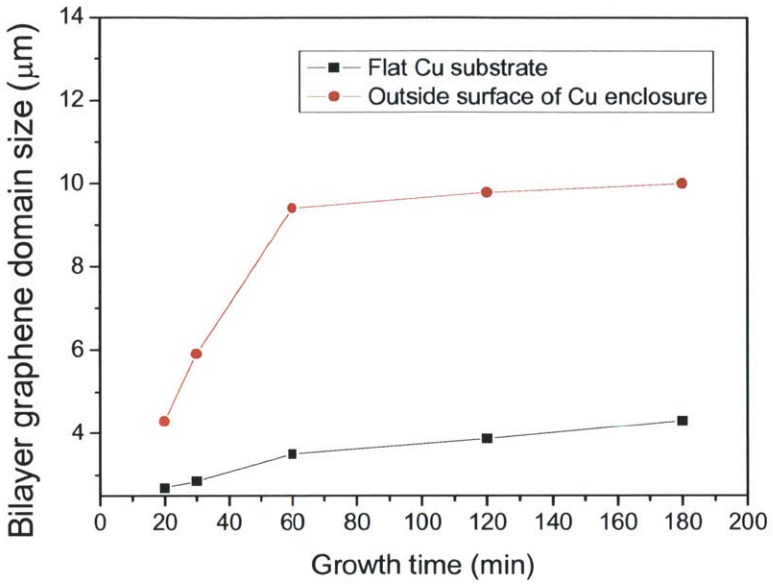

Figure 13. Comparison of the domain size of bilayer graphene on both flat Cu substrates and outside surface of Cu foil enclosures at 1000°C using 1.5sccm CH_4 and 35sccm H_2 as a function of time.

We plot the domain size of bilayer graphene on both flat Cu substrates and outside surface of Cu foil enclosures at 1000°C using 1.5sccm CH_4 and 35sccm H_2 as a function of time. It is clear that the domain size of bilayer on the outside is always larger than that on the flat Cu. Another interesting result we found is that the growth rate for bilayer graphene on the outside surface of Cu enclosure varies with time: the bilayer graphene grow at a faster rate for the first one hour after which the growth begins to saturate.

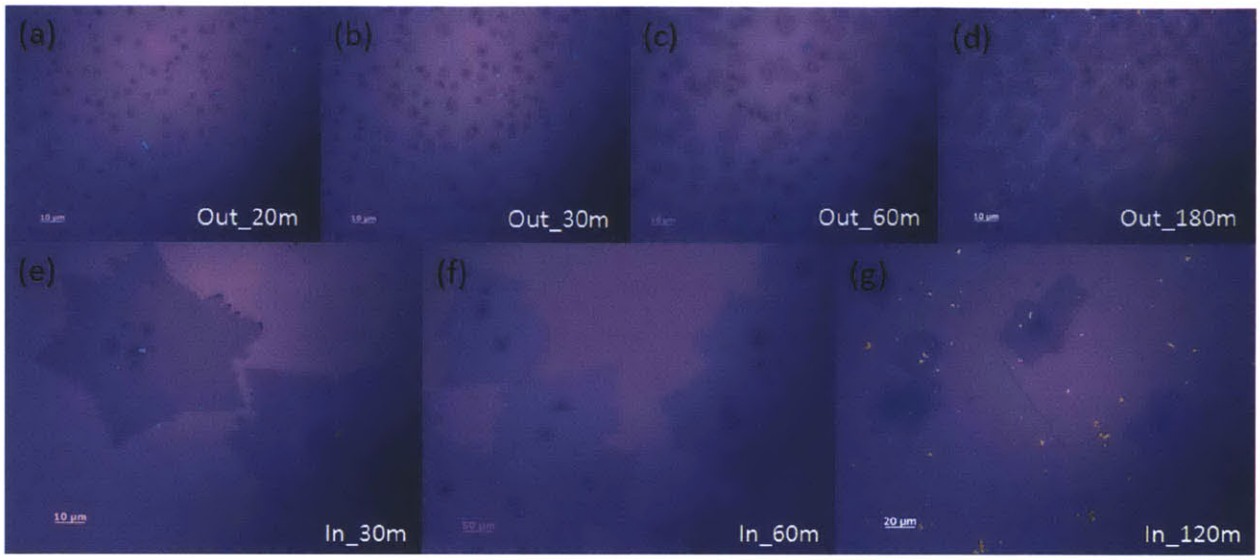

Figure 14. Optical images of graphene films grown on both inside and outside surface of Cu foil enclosures at 1000°C using 1.5sccm CH_4 and 35sccm H_2 as a function of time.

To reveal the growth mechanism, we studied the graphene grown on the inside surface of Cu foil enclosure at the same time. Figure 14a-d are the optical images of bilayer graphene films on the outside Cu foil enclosure, while figure 14e-g shows the corresponding graphene grown on the inside surface. In Figure e and f, there are large monolayer graphene domains on the inside surface of Cu enclosure. The inside surface of Cu substrate is not fully covered yet because of the extremely low carbon concentrations inside the enclosure. While in Figure g, we could observe a complete monolayer graphene with some bilayer and multi-layer domains after one hour growth. From those results obtained, we proposed that the growth rate of the bilayer graphene on the outside surface may be related to the interior surface of the enclosure. It seems that when the inside Cu surface is still exposed, the growth rate for bilayer graphene on the outside surface is much higher, compared to that once the inside surface is fully covered by monolayer graphene.

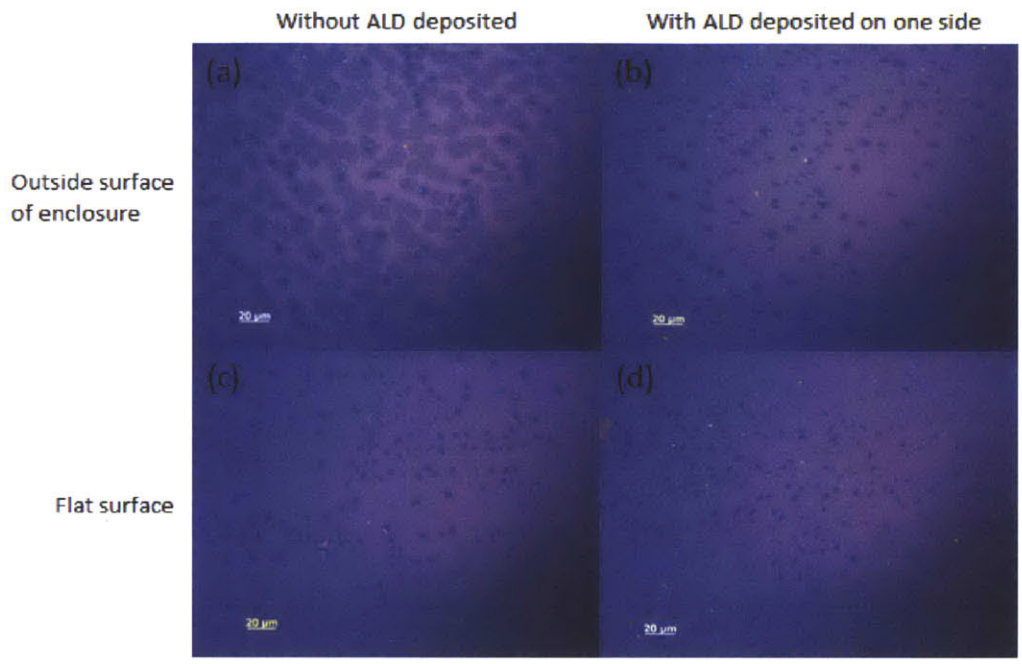

Figure 15. Optical images of graphene grown on bare flat Cu substrate, bare Cu foil enclosure, flat Cu substrate with one side deposited with Al_2O_3, Cu foil enclosure with inner side deposited with Al_2O_3.

Furthermore, we deposited Al_2O_3 by Atomic Layer Deposition (ALD) (10nm thick, deposited at 125°C) as a passivation layer on one side of Cu foil. One side of Cu foil was coated by PMMA using the same method as we transferred graphene to protect the surface from the deposition of Al_2O_3. After the deposition process, we removed the PMMA layer by acetone to expose the Cu surface. Under growth condition, the amorphous Al_2O_3 transforms into crystalline Al_2O_3. There is no graphene grown on the surface with Al_2O_3 deposited due to the presence of passivation layer and the passivation layer is not detrimental to the graphene growth on the non-passivated side. Four different types of Cu substrate were used: bare flat Cu substrate, bare Cu foil enclosure, flat Cu substrate with one side deposited with Al_2O_3, and Cu foil enclosure with inside surface deposited with Al_2O_3. After growth process at 1000°C for 2 hours in atmosphere of

1.5sccm CH_4 and 50sccm H_2, bilayer graphene in Figure 15a is much bigger on the outside surface. In contrast, the bilayer graphene in b is similar to that on the flat substrate in c and d. It should be noted that the Cu enclosure fails to give larger bilayer graphene on its outside surface when there is a passivation layer on the inside surface. Thus we believe the inside surface of the Cu enclosure plays a critical part for bilayer graphene formation on the outside surface and more work is needed to understand the underlying mechanism. We hypothesize the exposed Cu foil on the inside surface may have some catalytic effect on the bilayer on the other side of enclosure or it provides a pathway for the diffusion of carbon source to go through the thickness of Cu foil to help formation of bilayer graphene. There is obvious difference between bilayer graphene on bare flat Cu substrate and flat Cu substrate with one side deposited with Al_2O_3 because the complete monolayer graphene grows very fast (~5min). While for the enclosure structure, the insides environment is "sealed" so that it takes much longer time for monolayer graphene to fully cover the inside surface (> 1hour), which delays the "passivation" process and gives more time for bilayer growth.

In order to thoroughly understand the growth environment on the graphene growth, we have also tried layered Cu enclosures by putting a flat Cu substrate and a smaller Cu enclosure inside a bigger one. Figure 16a shows schematics of the layered enclosures structure from the cross sectional view.

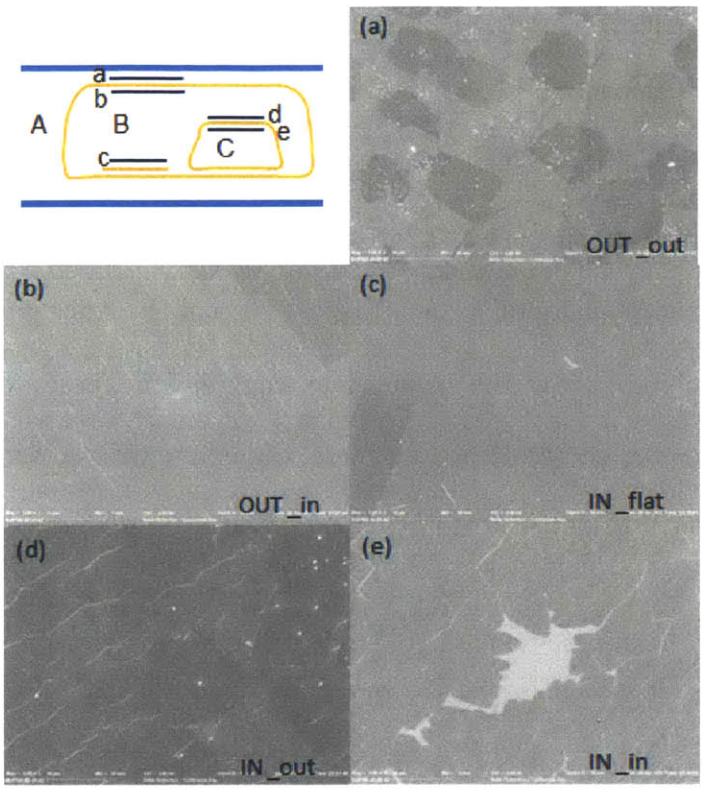

Figure 16. The schematics of the layered enclosure structure from the cross sectional view and the Scanning Electron Microscope (SEM) images of the graphene films on different surfaces of the structure.

There is three compartments denoted as A, B, C and five surfaces marked as a, b, c, d, e. As shown in Figure 16 above, the outside surface of smaller Cu enclosure (d), the inside surface of bigger Cu enclosure (b) and the flat substrate inside the bigger Cu enclosure (c) are in the same environment. However, only on the outside surfaces of both Cu enclosures we could observe bilayer graphene in Figure (a) (d). From this experiment, we learned that the effect of the environment plays a small role towards the growth of bilayer graphene.

3.1.2 Effect of Thickness

To study the effect of thickness, 99.9% purity Cu foil with thickness of 127um, 254um and 675um were used. Flat substrates were used here since it is difficult to form enclosures using thick Cu foil. Growth of graphene was carried out at 1000°C for 30 min and at 1050°C for another 90 min in the atmosphere of 3sccm CH_4 and 70sccm H_2. After growth, the furnace was turned off immediately to allow the samples to cool down. These studies show that the "nucleation density" and coverage of bilayer increases with thickness. We also observed much thicker films shown in (c), which is similar to graphene film grown using Ni thin film as a substrate.

Figure 17. Optical images of graphene films grown on 1 inch by 1 inch 99.9% Cu foil with thickness of 127um, 254um and 675um, respectively. The arrows show the location of thicker graphene films.

The dissolution and precipitation of carbon may account for the much thicker film. Thus we carry out a simple calculation for the maximum number of graphene layers on Cu foil by dissolution and precipitation.

For a Cu substrate with width (W):1.5cm, length(L): 1.5cm and thickness (T): 675um,

$$\rho_{Cu} = 8.9\ g/cm3,\ M_{Cu}=63.5g/mol$$

Solubility of carbon in Cu is about $4x10^{-6}$ in mole fraction at 1050°C, [34]

Volume of Cu foil: V=WLT and area of Cu foil: S_{Cu}=WL

Mass of dissolved Carbon in Cu foil: $Mc= 4x10^{-6} x\ \rho Vx12/63.5=1.02\mu g$

For one graphene hexagon, the distance between two carbon atoms is:

$$a = 1.42\ Å$$

The area for one hexagon can be expressed as:

$$S_{Hexagon} = 3\sqrt{3}/2a^2$$

Every hexagon contains two carbon atoms in the hexagonal lattice, so the number of carbon atoms N_C need to form a single layer is

$$N_C = 2\ x\ S_{Cu}/S_{Hexagon}=3.49x10^{16}$$

Mass for one graphene layer:

$$N_C/N_A\ x12.01=0.696\mu g$$

Then number of layers: 1.02/0.696 ~ 1.465 layers

From the number obtained above, we conclude that precipitation is no longer negligible when the Cu foil is thick regardless of the low solubility of carbon in Cu. We propose under the certain growth condition (high growth temperature), by tuning the thickness of Cu foil, the amount of

carbon source can be controlled. Therefore for a Cu foil with same surface area, the layer number of graphene should be determined by the precipitation of carbon from Cu foil with various thicknesses.

3.1.3 Effect of the Purity of Copper Foil

It is well known that impurities existing on the as-received copper foil act as nucleation sites for graphene growth. The impurities are suggested to possess a much lower nucleation barrier at the early stage of graphene growth, where the carbon sources first react and form seeds to grow larger graphene. Hence it is desirable to reduce the number of nucleation sites to prepare large size graphene domains. Several methods have been reported to effectively reduce the impurities and smooth the surface of the substrate such as electrical chemical polishing, chemical mechanical polishing (CMP) and long (up to 3 hours) pre-growth annealing. In this report a quick cleaning process (shown in Figure 18) is employed before growth to reduce impurities and thus increase the bilayer domain size and improve the uniformity of grown graphene film: Cu foil is dipped into commercially available Ni etchant (nitric acid, purchased from Transene company) for 30 seconds, immediately followed by rinsing using DI water. Although the surface is much rougher than before the cleaning process, the pre-growth substrate annealing step at 1000^{o}C for 30min helps smoothen out the rough surface.

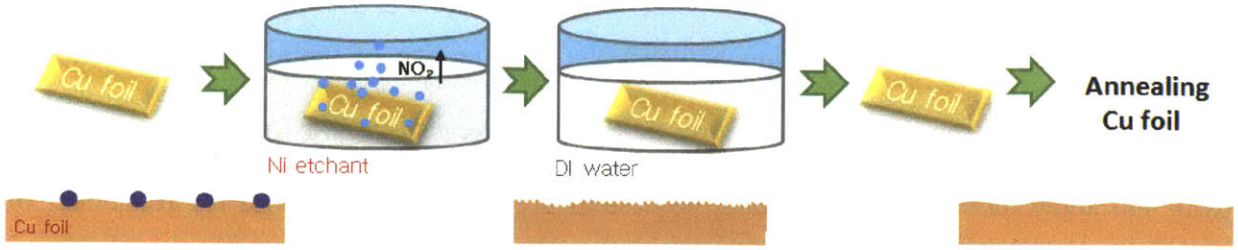

Figure 18. Procedure for Ni etchant cleaning process

Figure 19. Optical images of graphene films grown on the outside surface of the Cu foil enclosure for 2hour at 1035C using 1.5sccm CH4 and 35sccm H2: (a) 25um 99.8% Cu foil with Ni etchant cleaning; (b) 127um 99.9% Cu foil without and (c) with Ni etchant cleaning.

Figure 19 shows the optical images of graphene films grown on the outside surface of the Cu foil enclosure for 2hour at 1035°C using 1.5sccm CH_4/35sccm H_2. There is a background monolayer graphene in all the figures and the hexagonal shape indicates bilayer graphene. From the different color contrast in Figure a, the graphene films grown on Cu foil with low purity (99.8%) shows poor uniformity due to the presence of large numbers of impurities compared to (b), which is grown on 99.9% Cu foil. Based on Figure b and c, it is quite clear that the domain size in c (~16um) is much bigger than that in b (~8um). Based on the results above, we assume that the bilayer graphene films nucleate at the same location as the monolayer graphene. Therefore,

we attribute larger bilayer graphene domain size to lower nucleation density at the early stage of growth. More work on the correlation between the domain size of monolayer graphene and bilayer graphene will be discussed in more detail later. We use 99.9% Cu foil enclosure for growth and apply the Ni etchant cleaning process as pre-growth treatment for the remainder of this report.

3.2 Effect of the gasses

3.2.1 Methane

According to Li et al., low CH_4 concentration leads to a reduction of graphene nucleation, thus resulting in larger graphene domain size. CH4/H2 ratio of 0.7sccm/17.5sccm, 1.5sccm/35sccm, and 3sccm/70sccm was used for growth at 1035°C for 2hours.

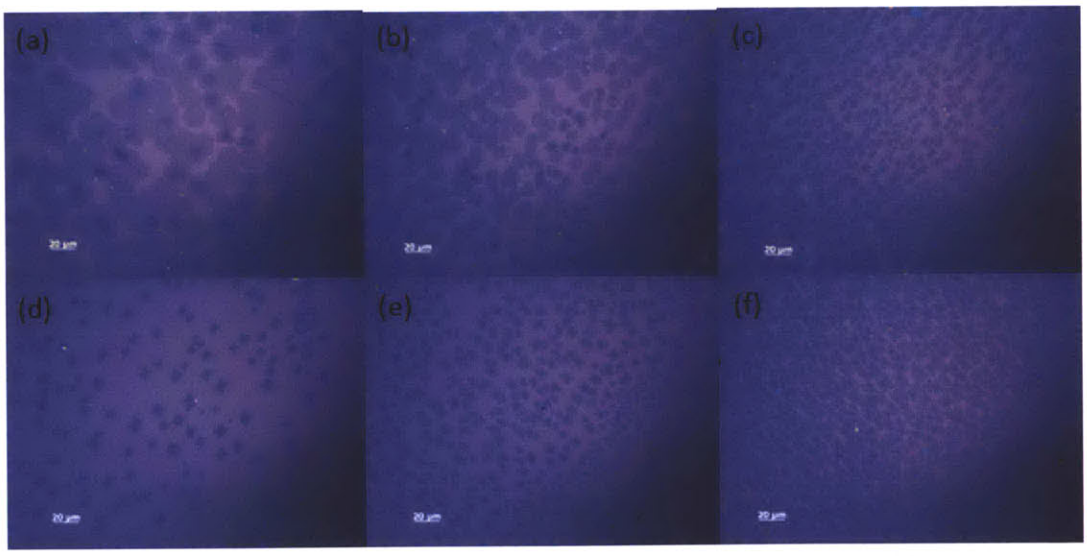

Figure 20. The graphene grown at 1035°C for 2hours using fixed CH4 to H2 ratio: 0.7sccm/17.5sccm, 1.5sccm /35sccm, 3sccm /70sccm.

The average domain size of bilayer graphene shown in Figure (a), (b), (c) is about 12μm, 8μm and 4μm respectively. When the flow rate of CH_4 is reduced, the domain size of bilayer graphene gets larger significantly. As mentioned earlier, we expect that the domain size of the bilayer may be related to the domain size of the monolayer. To confirm that, corresponding incomplete growth of monolayer graphene films using the same condition is for a growth period of 1 min are presented in (d), (e), and (f). It is clearly shown that the domain size of bilayer is strongly correlated with the domain size of monolayer: low methane flow rate leads to less nucleation density, hence resulting in larger domain size of both monolayer and bilayer graphene. However at the same time, multi-layers start to appear when the CH_4 flow rate decreases, as shown in Figure a.

We would like to address the importance of methane flow rate at the nucleation stage. In FigureX, graphene films grown at 1050°C using 0.7sccm CH_4 and 25sccm H_2 for two hours gives very low nucleation density but multilayer growth. The domain size of bilayer graphene is larger than 20μm. This condition is defined as condition a. While at the same temperature and for same growth time, graphene films grown using 1.5sccm CH4 and 10sccm H_2, shown in Figure 21 gives high nucleation density and smaller bilayer graphene domain size but negligible third or fourth graphene layer growth. This is noted as condition b. We combined these two conditions to do a two-step growth: using condition a to grow until the growth of monolayer graphene completes, then applying condition b for the rest of growth period, which in total is 2 hours.

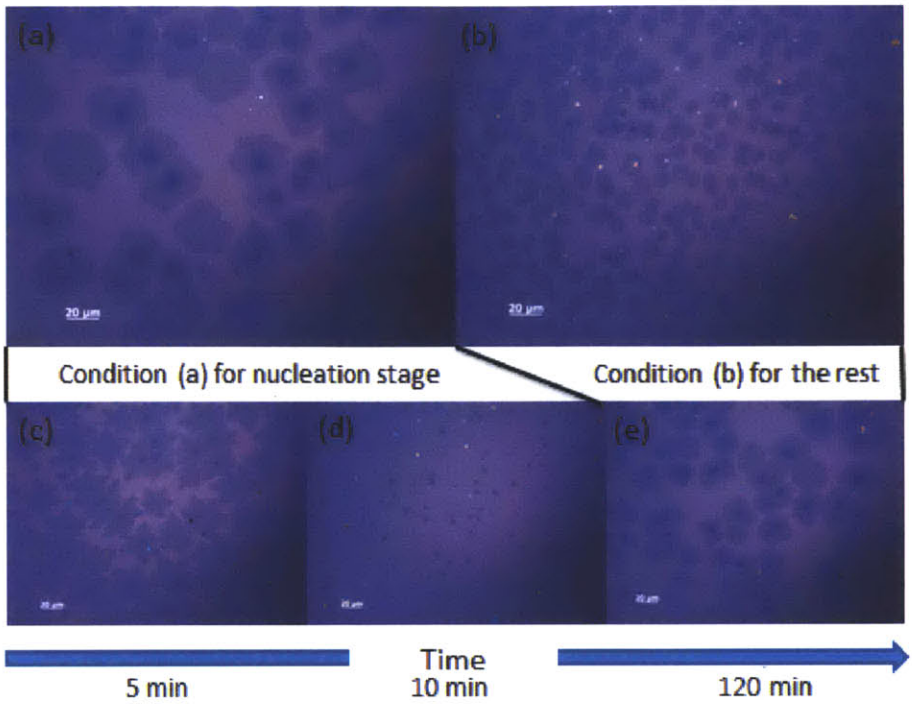

Figure 21. Optical Images of graphene films grown at 1050°C using 0.7sccm CH_4 and 25sccm H_2 (a) and 1.5sccm CH4 and 10sccm H_2 (b) for two hours. (c) and (d) shows graphene films using condition (a) for 5min and 10min while (e) shows the result after two-step growth.

From the figure above, by using condition a, the monolayer nucleates with larger domain size and completes growing at about 10 min. At the same time, we could observe small dots in d, which are the seeds for bilayer or multi-layers. After that, we immediately changed the growth condition to b for the rest of the growth time. Figure e shows the graphene film grown using two-step method and it is similar to figure a. It is important to point out that the condition at the early stage of growth determines the size of graphene domains regardless of the condition used for the growth period. Based on these results, we propose a two-step growth method by flowing low flow rate CH_4 at the early stages to get less numbers of nucleation densities, followed by a very rapid growth and emergence rate using a high CH_4 concentration in order to control the

nucleation stage to get a large graphene domain size while controlling the uniformity at the same time.

3.2.2 Effect of Hydrogen

On flat substrate, the size of bilayer is small and it is very hard to quantify the domain size and the density. It is not easy to neither draw any conclusion from the bilayer on flat substrate nor study the effect of the CH_4/H_2 ratio.

During the annealing process, hydrogen is used to reduce the thin oxide layer on the copper foil. In the growth stage, it has been reported that hydrogen plays a dual role: an activator of the surface bound carbon for graphene growth and an etching reagent that controls the size and morphology of the graphene domains. No graphene growth is observed when there is no hydrogen during the growth process.

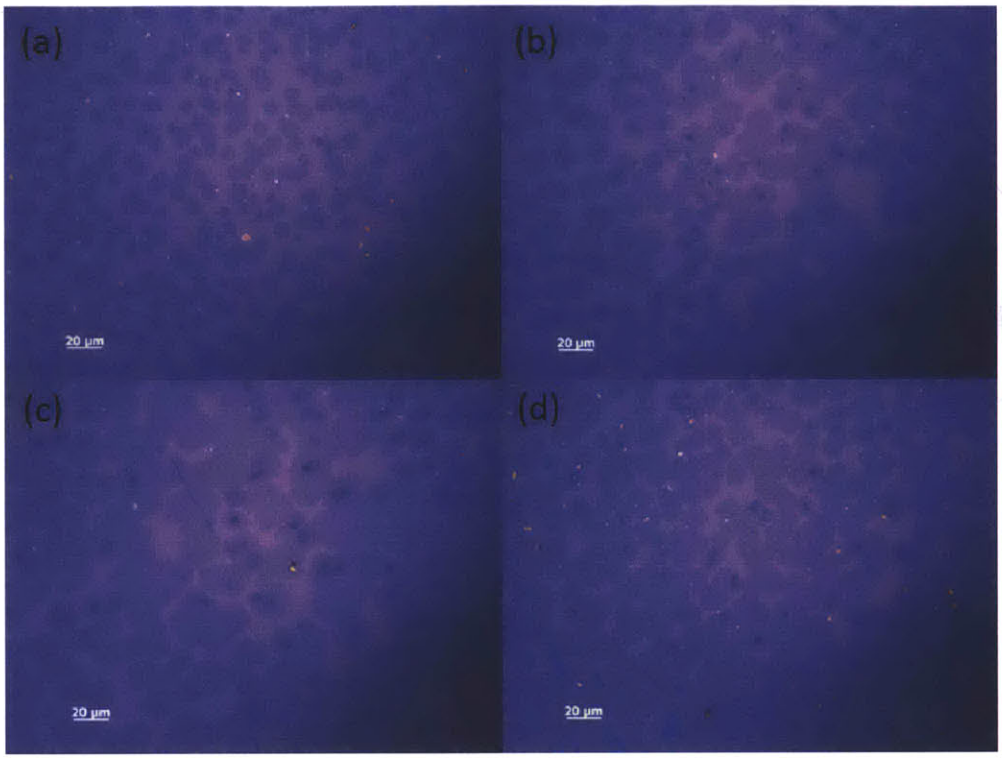

Figure 22, Optical images of graphene film grown on the outside surface of Cu foil enclosure using fixed CH_4 flow rate of 1.5sccm and varying the H_2 concentration of 10sccm (a), 35sccm (b), 50sccm (c) and 70sccm (d) at 1050°C for 2 hours.

In Figure 22, bilayer graphene films with nearly perfect hexagonal shapes are observed which we hypothesize could be related to high H_2 to CH_4 ratio. From Figure a-c, it clearly shows that with fixed CH_4 flow rate, a higher H_2 flow rate promotes the growth of larger bilayer graphene domains. However, as we further increase the H_2 flow rate, the domain size of bilayer graphene decreases.

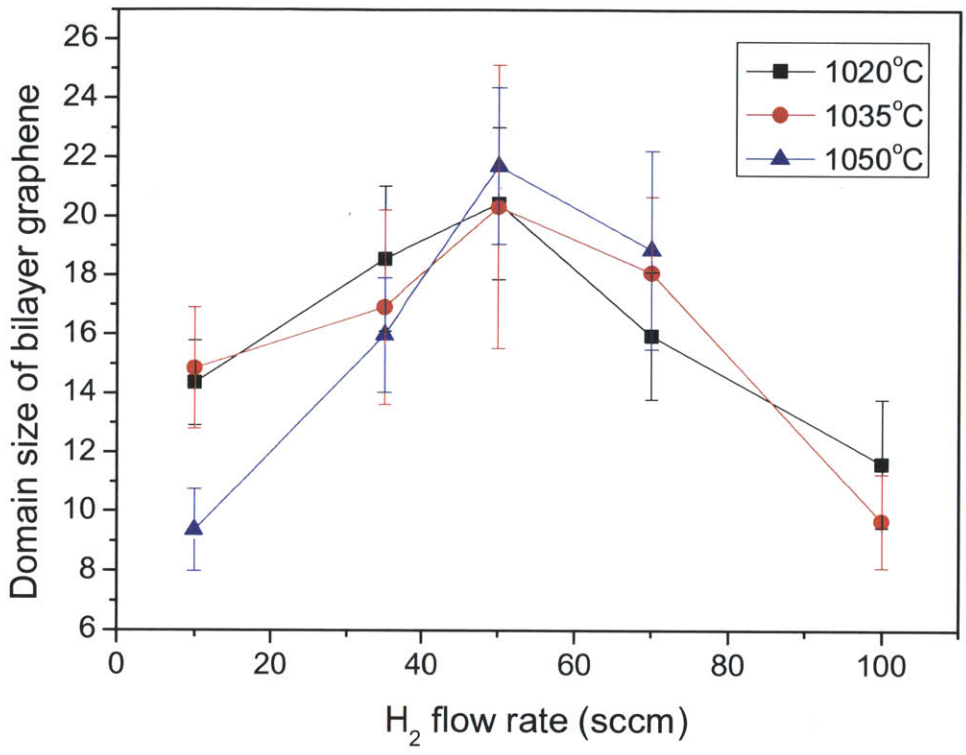

Figure 23. The domain size of bilayer graphene films as a function of H_2 flow rate with fixed CH_4 flow rate (1.5sccm) at 1020°C, 1035°C and 1050°C for 2hours.

We studied the domain size of bilayer graphene as a function of hydrogen flow rate at different temperatures. The domain size of bilayer graphene is measured from ten optical images taken at random spots from the various samples. Individual domain sizes vary a bit for each sample. Thus, to minimize statistical errors, 50 data points were used - 5 data points from each image – to calculate the average size. The analysis shows that for a fixed CH_4 flow rate, the bilayer domain size is maximal for H_2 flow rate of 50sccm. These results suggest that increasing H_2 flow rate increases bilayer domain size up to a certain point, beyond which domain size decreases again.

3.3 The effect of growth temperature

Figure 24. Optical images of graphene film grown on the outside surface of Cu foil enclosures using 0.7sccm CH_4/17.5sccm H_2) for 2 hours at 1000°C, 1035°C and 1050°C.

Figure24 shows that there is an optimized growth temperature (1035°C) for larger bilayer graphene. However from Figure 23 above on the study of H_2 flow rate, we could not draw any conclusions yet. There may be two reasons that explain the higher growth rate or larger bilayer graphene domain size: one is that higher temperature results in less nucleation density, thus larger domain size; the other reason may be that higher temperature helps either lower the energy barrier of bilayer graphene growth or decompose more CH_4 to accelerate the bilayer graphene growth.

3.4 The effect of total pressure

Figure 25. Optical images of graphene film grown on the outside surface of Cu foil enclosures at different total pressure (0.8 Tor, 1 Tor, 2 Tor for (a), (b), (c) respectively) using fixed CH_4 / H_2 flow rate (0.7sccm CH_4/17.5sccm H_2) at 1035°C for 2hours.

Figure 25 shows that with fixed CH_4 / H_2 flow rate, lower total pressure gives larger bilayer graphene domain size. We ascribe this observation to the less nucleation density under lower total pressure condition, which is consistent with previous report.

4. Characterization of Bilayer Graphene

4.1 Raman Spectroscopy

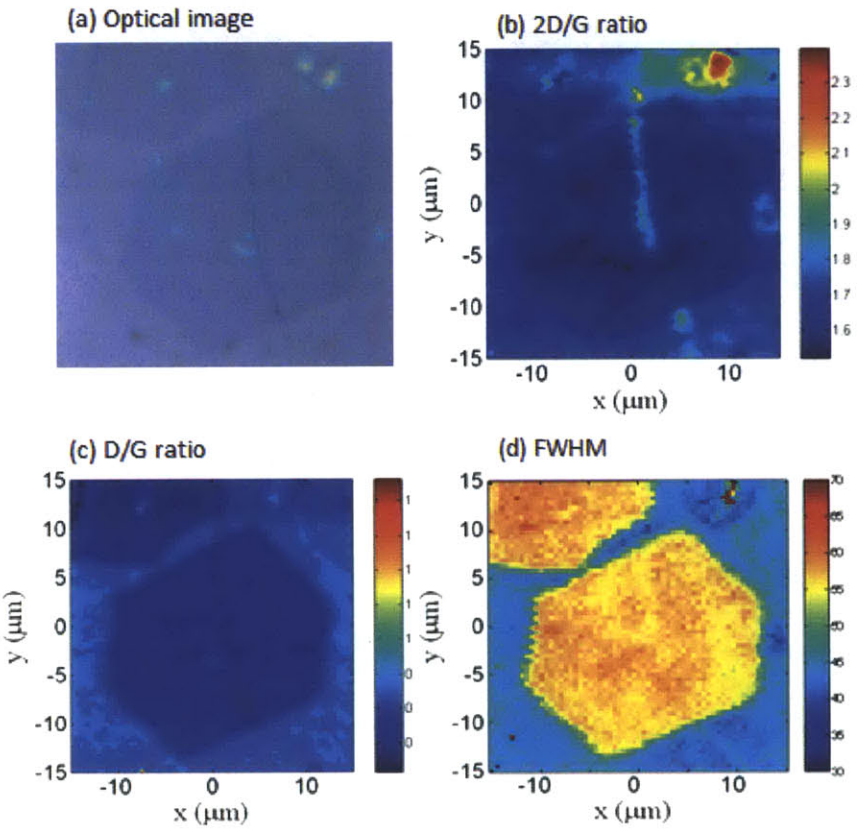

Figure 26. The optical image of graphene film transferred on the Si/SiO_2 substrate and Raman mapping of 2D/G, D/G ratio and FWHM.

Figure 26a shows an optical image of the graphene film transferred on the Si/SiO_2 substrate, indicating the presence of monolayer and bilayer regions. To probe the number of graphene

layers and obtain an initial assessment of layer stacking, the sample is characterized by Raman mapping using power lower than 0.1 mW.

Figure 26 b-d shows a representative mapping of the Raman 2D/G, D/G ratio and 2D band full width at half maximum (FWHM) acquired over a 30 × 30 μm^2 area. This data reveals the presence of bilayer domain with size of about 20μm on monolayer graphene background. Relatively low 2D/G ratios indicate the location of bilayer, which corresponds to the optical images in a. Also in figure c, the D/G ratio suggests that bilayer regions are less defective. The mapping of FWHM values are between 45 and 60 cm^{-1}.

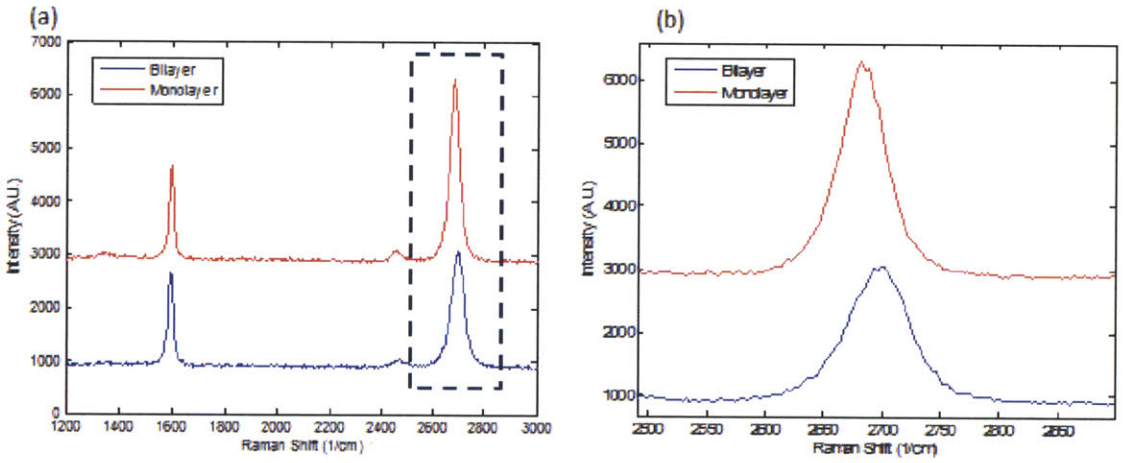

Figure 27. (a) Comparison of Raman spectra of monolayer and bilayer graphene transferred onto SiO_2/Si substrates. (b) Comparison of zoom-in 2D bands of monolayer and bilayer graphene.

Figure 27a shows a typical 532 nm laser excited Raman spectra taken from monolayer and bilayer graphene. The D bands (~1350 cm^{-1}), which correspond to defect level in graphene, are small in both spectra, which indicates that the graphene films are of high quality. In addition, the

D band in the Raman spectra for the bilayer is much smaller than that of the monolayer, as shown by the 2D/G mapping in Figure 26. More distinctive features arise at the 2D band located at ~2650 cm^{-1}. The spectrum of the monolayer region shows a narrow and symmetric 2D peak with the intensity ratio I_{2D}/I_G ~2 and full width at half-maximum (FWHM) of about 40 cm^{-1}. The 2D band for bilayer regions is generally wider with FWHM about 55 cm^{-1}. However, we did not observe the asymmetry, which indicates turbostratic stacking at this location.

4. Summary and Future Plan

In conclusion, we have investigated a novel method of growing bilayer graphene films on copper foil using LPCVD. The method is based on the copper "enclosure" described in this report. The bilayer domain size could reach as high as 50μm and the bilayer coverage could reach 90% before further optimization.

We found that the shape of enclosure plays a critical role in bilayer graphene formation on the outside surface. By carrying out time-dependent growth rate studies on the inside and outside surfaces of Cu foil enclosure, experimenting with ALD passivation layers, and investigating the effects of the layered enclosure structure, we ascribe this phenomenon to the effects of the inside surface, not the growth environment inside the enclosure.

We have also shown that the domain size of bilayer graphene is strongly correlated with the domain size of monolayer graphene, which itself is determined by the nucleation density at the early stages of growth. From the two-step growth study, we learned that by adjusting the CH_4 flow rate at the nucleation stage, the domain size of bilayer graphene can be controlled; low CH_4 flow rates result in larger bilayer graphene domain size but relatively poor uniformity. Additionally, we discovered that there is an optimal CH_4/H_2 ratio to achieve maximal bilayer domain size.

More work is needed to optimize the growth of bilayer graphene and to characterize its quality, stacking order, and uniformity. Furthermore, additional studies are needed to understand and model the underlying mechanism for the formation of bilayer graphene. Firstly, we will use the

two-step growth method to further optimize the bilayer graphene growth by minimizing CH_4 flow rate at the early stages to reduce nucleation density and therefore achieve larger bilayer graphene domain size, followed by a very rapid growth and emergence rate using a high CH_4 concentration to maintain the uniformity. Secondly, we will use Raman spectroscopy to characterize more bilayer graphene regions and carry out TEM and SAED to determine the thickness and the stacking order of the graphene film. Most importantly, we will study the growth mechanism of bilayer graphene growth on the outside surface of Cu foil enclosure: whether the bilayer graphene grows on top or underneath the existing monolayer and from where the carbon source originates. In the future, we would like to introduce isotope labeling C^{13} after the complete monolayer growth on the outside surface for the growth of the second layer and study its location by Raman mapping to monitor the growth mechanism. It is known that for bilayer graphene, the layer at the bottom, which is in contact with the SiO_2, will be doped during the transfer process, where a heating procedure is always required to remove residuals of PMMA. Therefore, an upshift of the Raman peak could be observed for the doped graphene layer, which is to be determined as the underlying layer, while for the layer on the top, the doping effect is absent. By distinguishing the shift of Raman peaks, we will be able to ascertain the location of the second layer, which will be helpful for our understanding of bilayer graphene growth.

References

(1) Novoselov, K. S.; Geim, A. K.; Morozov, S. V.; Jiang, D.; Zhang, Y.; Dubonos, S. V.; Grigorieva, I. V.; Firsov, A. A. *Science* **2004**, 306, 666

(2) Novoselov, K. S.; Geim, A. K.; Morozov, S. V.; Jiang, D.; Katsnelson, M. I.; Grigorieva, I. V.; Dubonos, S. V.; Firsov, A. A. *Nature* **2005**, 438, 197.

(3) Zhang, Y. B.; Tan, Y. W.; Stormer, H. L.; Kim, P. *Nature* **2005**, 438, 201.

(4) Han, M. Y.; Ozyilmaz, B.; Zhang, Y. B.; Kim, P. *Phys. Rev. Lett.* **2007**, 98, 206805

(5) Lin, Y. M.; Dimitrakopoulos, C,; Jenkins K. A.; Farmer D. B.; Chiu H. Y.; Grill. A. *Science* **2010**, 327, 662.

(6) Schwierz, F. *Nat Nanotechnol* **2010**, 5, 487.

(7) Dong, X. C.; Shi, Y. M.; Huang, W.; Chen, P.; Li, L. J. *Adv Mater* **2010**, 22, 1649.

(8) Huang, Y. X.; Dong, X. C.; Shi, Y. M.; Li, C. M.; Li, L. J.; Chen, P. *Nanoscale* **2010**, 2, 1485.

(9) Kim, K. S.; Zhao, Y.; Jang, H.; Lee, S. Y.; Kim, J. M.; Kim, K. S. *Nature* **2009**, 457, 706.

(10) Wang, X,; Zhi, L.; Mullen, K. *Nano Lett* **2008**, 8, 323.

(11) Geim, A. K.; Novoselov, K. S. *Nature Materials* **2007**, 6, 183-191.

(12) Berger, C.; Song, Z. M.; Li, X. B.; Wu, X. S.; Brown, N.; Naud, C.; Mayou, D.; Li, T. B.; Hass, J.; Marchenkov, A. N.; Conrad, E. H.; First, P. N.; de Heer, W. A. *Science* **2006**, 312, 1191.

(13) Sutter, P. W.; Flege, J. I.; Sutter, E. A. *Nat. Mater.* **2008**, 7, 406.

(14) Eda, G.; Fanchini, G.; Chhowalla, M. *Nature Nanotechnol* **2008** 3, 270–274.

(15) Reina, A.; Jia, X. T.; Ho, J.; Nezich, D.; Son, H. B.; Bulovic, V.; Dresselhaus, M. S.; Kong, J. *Nano Lett.* **2009**, 9, 30–35.

(16) Kim, K. S.; Zhao, Y.; Jang, H.; Lee, S. Y.; Kim, J. M.; Kim, K. S.; Ahn, J. H.; Kim, P.; Choi, J. Y.; Hong, B. H. *Nature* **2009**, 457, 706–710.

(17) Li, X. S.; Cai, W. W.; An, J. H.; Kim, S.; Nah, J.; Yang, D. X.; Piner, R.; Velamakanni, A.; Jung, I.; Tutuc, E.; Banerjee, S. K.; Colombo, L.; Ruoff, R. S. *Science* **2009**, 324, 1312–1314

(18) Liu, N.; Fu, L.; Dai, B. Y.; Yan, K.; Liu. X.; Zhao, R. Q.; Zhang, Y. F.; Liu, Z. F. *Nano Lett.* **2011**, 11, 297-303.

(19) Reina, A.; Thiele, S.; Jia, X. T.; Bhaviripudi, S.; Dresselhaus, M. S.; Schaefer, J. A.; Kong, J. *Nano Res.* **2009**, 2, 509–516.

(20) Li, X. S.; Cai, W. W.; S. K.; Colombo, L.; Ruoff, R. S. *Nano Lett,* **2009**, 12, 4268–4272

(21) Ohta, T.; Bostwick, A.; Seyller, T.; Horn, K.; Rotenberg, E. *Science* **2006**, 313, 951

(22) Oostinga, J. B.; Heersche, H. B.; Liu, X.; Morpurgo, A. F.; Vandersypen, L. M. K. *Nat. Mater.* **2008**, 7, 151.

(23) Zhang, Y.; Tang, T.-T.; Girit, C.; Hao, Z.; Martin, M. C.; Zettle, A.; Crommie, M. F.; Shen, Y. R.; Wang, F. *Nature* **2009**, 459, 820.

(24) Banerjee, S. K.; Register, L. F.; Tutuc, E.; Reddy, D.; MacDonald. A. H. *IEEE Electron Device Lett.* **2009**, 20, 158-160.

(25) Suk, J. W.; Kitt, A.; Magnuson, C. W.; Hao, Y. F.; Ahmed, S.; An, J. H.; Swan, A. K.; Goldberg, B. B.; Ruoff, R. S. *ACS Nano*, **2011**, 5 (9), 6916–6924.

(26) Li, X. S.; Zhu, Y. W.; Cai, W. W.; Borysiak, M.; Han, B. Y.; Chen, D.; Piner, R. D.; Colombo. L.; and Ruoff, R. S. *Nano Lett*, **2009**, 9 (12), 4359-4363.

(27) Yan, K.; Peng, H. L.; Zhou, Y.; Li, H,; Liu, Z. F. *Nano Lett*, **2011**, 11, 1106–1110.

(28) Xia, F.; Farmer, D. B.; Lin, Y.-m.; Avouris, P. *Nano Lett.* **2010**, 10, 715.

(29) Li, X. S.; Cai, W. W.; Colombo, L. G.; Ruoff, R. S. *Nano Lett.* **2009**, 9, 4268-4272.

(30) Lee, S.; Lee, K.; Zhong, Z. H. *Nano Lett.* **2010**, 10, 4702-4707.

(31) Liu, X.; Fu, L.; Liu, N.; Gao, T.; Zhang, Y. F.; Liao, L.; Liu, Z. F. *J. Phys. Chem. C* **2009**, 115, 11976-11982.

(32) Nie, S.; Walter, A. L.; Cartelt, N. C.; Starodub, E.; Bostwick, A.; Rotenberg, E.; McCarty, K. F. *ACS Nano*. **2011**, 5 (3), 2298–2306

(33) Nie, S.; Wu, W.; Xing, S. R.; Yu, Q. K.; Pei, S. S.; McCarty. K. F. *Physical Review B*. **2012**. submitted

(34) Lopez, G. A.; Mittemeijer, E. J. *Scripta Meaterialia*. **2004**. 51. 1-5